

## MIT Open Access Articles

*The REgolith X-Ray Imaging Spectrometer (REXIS) for OSIRIS-REx: identifying regional elemental enrichment on asteroids*

The MIT Faculty has made this article openly available. **Please share** how this access benefits you. Your story matters.

**Citation:** Allen, Branden, Jonathan Grindlay, Jaesub Hong, Richard P. Binzel, Rebecca Masterson, Niraj K. Inamdar, Mark Chodas, et al. "The REgolith X-Ray Imaging Spectrometer (REXIS) for OSIRIS-REx: Identifying Regional Elemental Enrichment on Asteroids." Edited by Mark A. Kahan and Marie B. Levine. Optical Modeling and Performance Predictions VI (September 27, 2013). © 2013 SPIE

**As Published:** <http://dx.doi.org/10.1117/12.2041715>

**Publisher:** SPIE

**Persistent URL:** <http://hdl.handle.net/1721.1/85182>

**Version:** Final published version: final published article, as it appeared in a journal, conference proceedings, or other formally published context

**Terms of Use:** Article is made available in accordance with the publisher's policy and may be subject to US copyright law. Please refer to the publisher's site for terms of use.



# The REgolith X-Ray Imaging Spectrometer (REXIS) for OSIRIS-REx: Identifying Regional Elemental Enrichment on Asteroids

Branden Allen<sup>a</sup>, Jonathan Grindlay<sup>a</sup>, Jaesub Hong<sup>a</sup>, Richard P. Binzel<sup>b</sup>, Rebecca Masterson<sup>c</sup>,  
Niraj K. Inamdar<sup>b,c</sup>, Mark Chodas<sup>c</sup>, Matthew W. Smith<sup>c</sup>, Marshall W. Bautz<sup>d</sup>,  
Steven E. Kissel<sup>d</sup>, Joel Villasenor<sup>d</sup>, Miruna Oprescu<sup>a</sup>, Nicholas Induni<sup>a</sup>,

<sup>a</sup>Harvard College Observatory, 60 Garden Street, Cambridge, MA 02138, USA

<sup>b</sup>Department of Earth, Atmospheric, and Planetary Sciences, Massachusetts Institute of  
Technology, Cambridge, MA 02139, USA

<sup>c</sup>Space Systems Lab, Massachusetts Institute of Technology, Cambridge, MA 02139, USA

<sup>d</sup>Kavli Institute for Astrophysics and Space Research, Massachusetts Institute of Technology,  
Cambridge, MA 02139, USA

## ABSTRACT

The OSIRIS-REx Mission was selected under the NASA New Frontiers program and is scheduled for launch in September of 2016 for a rendezvous with, and collection of a sample from the surface of asteroid Bennu in 2019. 101955 Bennu (previously 1999 RQ<sub>36</sub>) is an Apollo (near-Earth) asteroid originally discovered by the LINEAR project in 1999 which has since been classified as a potentially hazardous near-Earth object. The REgolith X-Ray Imaging Spectrometer (REXIS) was proposed jointly by MIT and Harvard and was subsequently accepted as a student led instrument for the determination of the elemental composition of the asteroid's surface as well as the surface distribution of select elements through solar induced X-ray fluorescence. REXIS consists of a detector plane that contains 4 X-ray CCDs integrated into a wide field coded aperture telescope with a focal length of 20 cm for the detection of regions with enhanced abundance in key elements at 50 m scales. Elemental surface distributions of approximately 50-200 m scales can be detected using the instrument as a simple collimator. An overview of the observation strategy of the REXIS instrument and expected performance are presented here.

## 1. THE OSIRIS-REX MISSION

The **O**rigins, **S**pectral Interpretation, **R**esource Identification, **S**ecurity, **R**egolith, **E**xplorer (OSIRIS-REx) [1, 2] is a multifaceted asteroid regolith sample return mission chosen as part of NASA's New Frontiers Program for the characterization of a 101955 Bennu (previously designated 1999 RQ<sub>36</sub>). OSIRIS-REx is equipped with 5 separate instruments:

1. The **OSIRIS-REx Camera Suite** (OCAMS) which consists of three separate visible telescopes for the mapping and sample site selection on the asteroid at visible wavelengths [3].
2. The **OSIRIS-REx Laser Altimeter** (OLA) which utilizes scanning LIDAR to provide high resolution topographical measurements of the asteroid surface [4].
3. Characterization of the asteroid spectra at visible and infrared wavelengths will be carried out using the **OSIRIS-REx Visible and IR Spectrometer** (OVIRS) [5, 6].
4. Thermal emission spectral maps will be provided by the **OSIRIS-REx Thermal Emission Spectrometer** (OTES).
5. The **REgolith X-Ray Imaging Spectrometer** (REXIS) will determine the global elemental abundances and search for anisotropies in the composition of Bennu.

---

Further author information: (Send correspondence to Branden Allen; E-Mail: [ballen@cfa.harvard.edu](mailto:ballen@cfa.harvard.edu))

The spacecraft also carries the **Touch-And-Go Sample Acquisition Mechanism (TAGSAM)** for the retrieval of no less than 60 g of regolith from the surface of Benu.

The purpose and primary objectives of the OSIRIS-REx mission are the return of a regolith sample, the global characterization of the asteroid's morphology and composition, measurement of the properties of the sample site at sub-centimeter scales, and threat assessment with regard to potential future impacts with the Earth. The threat assessment will be carried out by performing a field Yarkovsky test which will be used to refine future orbital projections. Aside from its power to extinguish life Benu is also potentially important for advancing our understanding of planet formation, in particular our understanding of the origin of organic material which is of fundamental importance for the development of life on Earth (see §2). The measurements made in orbit will also be used to cross-calibrate observations carried out from the vicinity of the Earth which should contribute to added precision in the measurement of asteroid properties in general.

OSIRIS-REx is scheduled for launch in September of 2016, with a backup date scheduled one year later. After a gravity assist maneuver with the Earth in late 2017 OSIRIS-REx will enter the asteroid approach phase in late 2019 and carry out a preliminary survey for small natural satellites which could pose a danger to the mission. Once it is determined to be safe to proceed OSIRIS-REx will settle into an orbit around Benu and primary science operations will commence. Observations with the REXIS (see §3) will be performed in orbital phase B at a nominal altitude of 720 m above the surface of the asteroid in order to assist with the selection of potential sample retrieval sites by characterizing the global elemental abundance of Benu and searching for regions of anomalous composition. After selection of a sample site OSIRIS-REx will descend to the surface of Benu and collect up to 2.2 kg of regolith. OSIRIS-REx will depart the asteroid in March of 2021 with its cargo which will land with the sample return capsule (SRC) at the Utah Test and Training Range (UTTR) in September of 2023.

## 2. TARGET: NEAR EARTH ASTEROID 101955 BENNU

101955 Benu (1999 RQ<sub>36</sub>), was selected by the OSIRIS-REx team for its accessibility, relatively high impact probability, and it is a B-Type asteroid: a class that likely samples the early chemistry of the solar system.

Benu was originally detected by the Lincoln Near-Earth Asteroid Program (LINEAR) in 1999 [7] and subsequently was determined to have the highest impact hazard rating based on the Palermo Technical Scale (c.f. [8]) with a cumulative value of  $-1.12$  and a maximum value of  $-1.52$ ; for comparison the median values drawn from a sample of 444 asteroids currently tracked by the JPL Sentry System are  $P_{\text{cumulative}} = -6.225 \pm 1.490$  and  $P_{\text{maximum}} = -6.545 \pm 1.474$  where the errors stated here are the RMS values calculated over the sample [9]. The cumulative impact probability with the Earth is  $7.1 \times 10^{-4}$  with 8 potential impacts between 2169 and 2199. The orbit of Benu is in a pseudo-resonance with the Earth's orbit and consequently makes close passes at intervals of approximately 6 years; since its discovery ground based radar observations have been performed during the close encounters of 1999, 2005 and 2011 allowing for detailed characterization of the gross dimensions. From these measurements it has been determined that Benu possesses a mean diameter of  $492 \pm 20$  m with a total volume of  $0.0623 \pm 0.006$  km<sup>3</sup> and a surface area of  $0.786 \pm 0.04$  km<sup>2</sup> (see figure 1) [10]. The shape of the asteroid is roughly spherical with a top-like appearance and a maximum diameter of  $565 \pm 10$  m. From the same observations the sidereal rotation period was determined to be  $4.297 \pm 0.002$  hours and that the asteroid has a bulk density of  $0.98 \pm 0.15$  g/cm<sup>3</sup> [11].

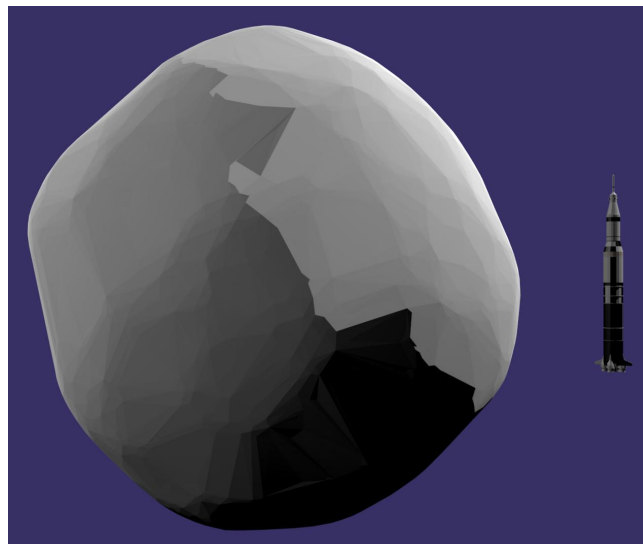


Figure 1: A comparison of 101955 Benu with the Saturn 5 rocket. Benu has a mean radius of  $246 \pm 10$  m, the Saturn 5 had a height of 110 m.

Instrument	Target	Obs. Start Obs. End	Eng. Rng. [keV] Eng. Res. [keV]	Det. Area [cm <sup>2</sup> ] FOV	Notes
Apollo 15 XRFS	Moon	30.7.1971 4.8.1971	1.5-5.5 —	25.0 30.0°	3 collimated prop. counters [13, 14]
Kaguya-XRS <sup>•</sup>	Moon	14.9.2007 29.5.2009	1.0-10.0 0.180@5.9 keV	100.0 12.0° × 12.0°	4 collimators each with 2 × 2 CCDs (Rad. Damage) [15–17]
Hayabusa-XRS	25143 Itokawa	12.9.2005 24.11.2005	1.0-10.0 0.14@1.5 keV	25.0 3.5° × 3.5°	1 collimator with 2 × 2 CCDs [18–20]
Chandrayaan-1 C1XS	Moon	11.2008 8.2009	0.8-20.0 0.2	24.0 12.0°	24 SCDs in 3 collimators [21, 22]
SMART-1 D-CIXS	Moon	3.2005 3.2005	1.0-20.0 0.2	12.0 12°	24 SCDs in 3 collimators [23]
NEAR-XRS	443 Eros	4.5.2000 10.2.2001	1.5-5.5 0.83@5.9 keV	25.0 5°	3 collimated prop. counters [24]
Mercury Messenger XRS	Mercury	2011 Present	1.0-10 0.88@5.9 keV	10.0 12.0°	3 collimated prop. counters [25, 26]
Bepicolombo MIXS-C <sup>†</sup>	Mercury	8.2019 8.2020	0.5-10.0 0.128@5.9 keV	3.68 10.4°	Single APS in a single collimator [27, 28]
Bepicolombo MIXS-T <sup>†*</sup>	Mercury	8.2019 8.2020	0.5-10.0 0.128@5.9 keV	3.68 1.1°	APS w/Focusing optic 6' angular res. [27, 28]
OSIRIS-REx REXIS <sup>‡</sup>	101955 Bennu	12.2019 3.2020	0.3-10.0 0.130@5.9keV	24.2 30.0°	2 × 2 CCDs Coded-aperture tel. 26.2' angular res.

<sup>•</sup>Radiation Damage

<sup>†</sup>Future Missions

<sup>‡</sup>Coded-Aperture Telescope

\*Focusing Telescope

Table 1: A list of previous remote sensing X-ray fluorescence experiments flown or scheduled to be flown for the characterization of elemental abundances on airless bodies within the solar system.

Asteroids constitute the remaining building blocks of terrestrial planet formation and therefore provide an important window into the conditions present during the formation of the Solar System. More specifically primordial carbonaceous asteroids are a potential source of organic matter and other volatile elements, such as sulfur, and may account for a large fraction of these elements on the Earth. Observations of Bennu are characterized by a low albedo of approximately  $0.035 \pm 0.015$  and a lack of absorption bands characterizing other B-Type asteroids; the closest meteorite analog was determined to be that of a C1 and/or CM1 Chondrite [12].

### 3. THE REGOLITH X-RAY IMAGING SPECTROMETER

The **RE**golith **X**-Ray **I**maging **S**pectrometer (REXIS) (shown in figure 2) was conceived as a student led project whose primary goal is the education of science and engineering students who will participate in the development of flight hardware in future space missions. Additionally REXIS also augments the observation capabilities of the OSIRIS-REx mission at the high end of the electromagnetic spectrum which will enable characterization



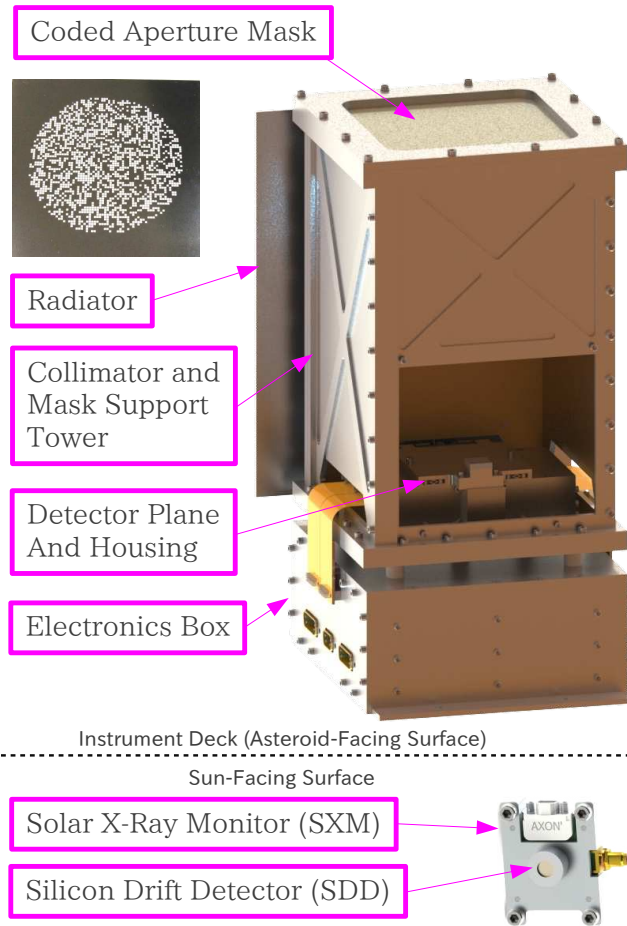


Figure 2: The REXIS instrument consists of the main detector and collimator assembly and the electronics box which are physically connected by 5 thermal isolation standoffs. The mating interface to the OSIRIS-REx spacecraft are located on the underside of the electronics box. Shown to the upper left is the prototype coded aperture mask which makes detection of elemental abundance enhancements at 50 m scales possible. The solar X-ray monitor (SXM) is mounted on the sun-facing side of the spacecraft separately from the primary telescope.

of the asteroid elemental abundances from a global scale down to 50 m, a capability unique to REXIS among instruments of this type that have previously flown (c.f. table 1).

REXIS is designed to observe induced X-ray fluorescence lines emitted from the asteroid surface that arise as a result of exposure to solar X-rays as well as the cosmic X-ray background (CXB). A number of previous missions have employed this technique for the observation of airless bodies throughout the Solar System beginning with the Apollo 15 X-ray fluorescence experiment for the observation of the moon [14]. More recent observations of the Moon have been carried out by the D-CIXS mapping spectrometer on SMART-1 [23], the C1XS on

Physical Parameters	
Total Mass (CBE)	4.4 kg
Total Power (CBE)	10.8 W
Focal Length	20 cm
Detector Plane	2 × 2 CCDs
Active Area	24.159 cm <sup>2</sup>
FOV	0.18 sr (30° circ.) (FWZI)
Angular Resolution	26.2' (5.6 m @ 730 m)
CCD Parameters	
Type	MIT-LL CCID-41
Energy Resolution	130 eV @ 5.9 keV
Energy Range	0.3-10.0 keV (QE≥0.3)
Pixels	1024 × 1024
Pixel Dimensions	24 μm × 24 μm
Active Area	6.03880 cm <sup>2</sup>
Super-Pixel Dimensions	0.192 mm × 0.192 mm
Depletion Depth	45 μm
Optical Blocking	220 nm Direct Deposited Al
Operating Temperature	≤ -60°C
Mask Parameters	
Thickness	100 μm
Composition	ASTI-301 Stainless Steel
Pattern Diameter	98.304 mm (64 Pixels)
Open Hole Fraction	0.5
Pixel Pitch	1.536 mm
Support Grid Width	100 μm
Solar X-Ray Monitor (SXM)	
Detector	Amptek XR-100 SDD
Active Area	5 mm × 5 mm
Energy Range	1-20 keV
Energy Resolution	125 eV @ 5.9 keV
Depletion Depth	500 μm
Optical Blocking	0.5 mil Be Window
Operating Temperature	≤ 0°C

Table 2: A summary of the critical instrument parameters for REXIS, the CCDs, the coded aperture mask and the solar X-ray monitor (SXM) shown to the left in figure 2. The values given for the mass and power consumption of the instrument are the current best estimates (CBE).

Chandrayaan-1 [21, 22, 29], and the XRS aboard Kaguya [15, 16]. Additionally similar observations of two separate asteroids 433 Eros and 25143 Itokawa have been carried out by the Hayabusa-XRS [19, 20] and NEAR-XRS [24] respectively, and the Mercury Messenger mission is currently in the process of mapping the elemental abundances on the surface of Mercury [26]. To date the instruments that have flown have all employed a collimator based instrument tuned to the specific orbital and target parameters imposed by the constraints of the individual missions (see table 1). This allows for some reconstruction of the elemental abundances as a function of position on the object under study, however the angular resolution is defined by the size of the collimator and is therefore rather coarse compared to what is achievable utilizing focusing X-ray optics or a coded-aperture instrument.

A variety of detector planes have been used in conjunction with these missions. To date XRF experiments flown by National Aeronautics and Space Administration (NASA): the Apollo 15 XRFS, NEAR-XRS, and the Mercury Messenger XRS have been limited to the use of essentially the same instrument consisting of 3 gas proportional counters (GPC) where one GPC is outfitted with an Al filter, another is outfitted with a Mg filter, and the third is simply equipped with a Be optical blocking filter in order to deconvolve the Al-K, Mg-K, and Si-K emission lines in spite of the poor energy resolution (880 eV @ 6.5 keV) of these detectors. More recent efforts supported by the Japanese Aerospace Exploration Agency (JAXA) have focused on the use of  $4 \times 4$  arrays of X-ray CCDs integrated into collimators and have the advantage of substantially improved energy resolution 140 eV @ 1 keV. The primary drawback of this method is the susceptibility of CCDs to radiation damage, in particular from low energy proton induced charge transfer inefficiencies (CTI), which prevented the success of one instrument: the Kaguya-XRS. Until recently the efforts of the European Space Agency (ESA) were focused on the use of swept charge devices (SCD) which are non-imaging silicon based detectors similar to a CCD but with an altered electrode layout optimized for rapid readout that have energy resolutions comparable to CCDs. The ESA Bepicolombo mission to Mercury, set to begin observations in August of 2019, will employ two XRF instruments: a telescope consisting of a collimator and a Depleted P-Channel Field Effect Transistor (DEPFET) array detector plane (MIXS-C) and an identical detector plane outfitted with a focusing optic (MIXS-T) [27, 28].

The primary REXIS instrument consists of a detector plane comprised of a  $2 \times 2$  array of back illuminated (BI) CCDs, MIT Lincoln Laboratory (LL) CCID-41, identical to those used in the X-Ray Imaging Spectrometer (XIS) [30] on Suzaku [31], a joint astrophysics mission between NASA and JAXA, which have quantum efficiencies greater than 0.75 between 0.4 and 6.0 keV (see figure 3) [32, 33]. The active area of the CCD is composed of a  $1024 \times 1024$  array of pixels with a pitch of  $24 \mu\text{m}$ . There is a gap of 38 detector pixels (0.912 mm) between the active areas of the individual CCDs to ensure the safe assembly of the detector plane which are aligned in order to preserve the pixel pitch across the entire detector plane. A optical blocking filter consisting of a 220 nm aluminium layer deposited directly on the CCD is present to mitigate the undesirable background signal that would otherwise be induced by optical/UV photons reflected from the surface of the asteroid and onto the detector plane. The detector plane is housed in a thermally isolated, shielded box which itself is located inside of the instrument main truss that supports a coded aperture mask located 20 cm above the detector plane. The detector plane is passively cooled to less than  $-60^\circ\text{C}$  by means of a radiator attached to one surface of the main truss and is oriented toward deep space during science operations. This entire assembly sits atop and is

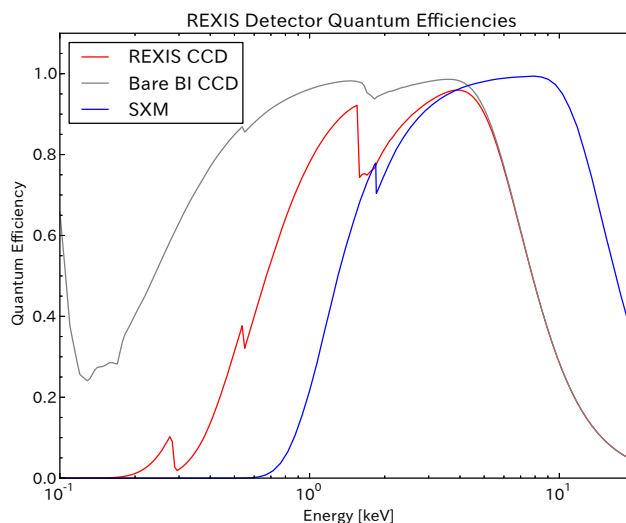


Figure 3: The on-axis quantum efficiency curve of the bare MIT Lincoln Laboratory CCID-41 and the predicted performance of the REXIS flight CCDs after application of the 220 nm thick Al optical blocking filter and taking into account the effects of molecular surface contamination between 0.1 and 20 keV. The solar X-ray monitor (SXM) quantum efficiency including the 0.5 mil thick Be optical blocking window is also shown.

affixed with low thermal conductivity standoffs to the REXIS electronics box which contains the instrument's support electronics. The mask itself is manufactured from a single piece of 100  $\mu\text{m}$  thick ASI-301 stainless steel with a random pattern of chemically etched open holes. The pitch of the individual mask elements is 1.536 mm with an open hole fraction of 0.5 and a support grid running between the individual elements of 100  $\mu\text{m}$ . The support grid reduces the throughput to 0.437. In order to guard against radiation induced CTI and preserve the spectral resolution of the detector plane the REXIS instrument will be outfitted with a radiation cover at the aperture which will remain closed until observations commence. The detector plane is also equipped with a number of  $^{55}\text{Fe}$  calibration sources which are arranged to enable the monitoring of a subset of detector pixels at the beginning and end of the CCD readout chain throughout observations of Bennu. The underside of the radiation cover, mounted above the coded aperture mask, also contains an additional series  $^{55}\text{Fe}$  sources which will be used to calibrate and monitor all pixels in the detector plane prior to the opening of the cover for science observations.

The solar X-ray spectrum is highly variable characterized by episodic flares and outbursts typically on 600 s timescale with longer durations on the order of days possible; on longer time scales changes in flux of up to 3 orders of magnitude is also possible. For this reason REXIS, as well as all other XRF experiments of this type, must be equipped with an additional sensor for the measurement of the local solar X-ray spectrum in order to properly interpret the data. To this end REXIS includes a separate solar X-ray monitor (SXM) which is attached to the sun-facing side of the spacecraft and interfaces directly with the REXIS main detector electronics. The SXM is constructed using a commercially available silicon drift detector (SDD) manufactured by Amptek read out by custom designed electronics originally commissioned for use in the Neutron Star Interior Composition Explorer (NICER) [34, 35] that have been optimized for use with the REXIS instrument. The SDD has an active area of 25  $\text{mm}^2$  and is housed behind a 0.5 mil thick optical blocking filter composed of Be. In order to maintain a nominal operating temperature less than 0°C under direct exposure from the sun a thermoelectric cooler is located directly beneath the SDD. The fully assembled SXM will have a quantum efficiency greater than 0.1 between 1.1 and 30.0 keV with an energy resolution of 125 eV at 5.9 keV (see figure 3) [35, 36].

The primary REXIS instrument in conjunction with the SXM will carry out observations of the asteroid Bennu and measure the asteroid elemental composition (see §6) and conduct a search for regions of enhanced abundance as described in §7.

#### 4. OBSERVATION STRATEGY

After an initial cruise phase and survey (see §1) the OSIRIS-REx spacecraft will enter a roughly circular polar terminator orbit with a radius of 1 km or  $730 \pm 20$  m above the surface of the asteroid with an orbital period of 27 hours. 11 hours of observation each day are currently allocated for nadir pointing observations during which time the REXIS field of view will be centered on the asteroid. The position of the REXIS-SXM has been optimized for this observation period so that the sun remains in the SXM field of view to enable continuous monitoring of the solar X-ray spectrum throughout science operations. Concordantly a radiator affixed to the main collimator and mask support structure for passive cooling of the CCDs to less than -60°C has been mounted so that it is oriented into deep space during these observations as well.

The CCDs in the detector plane are read out with an integration time of 4 seconds per frame, and a frame transfer time of 10 ms. The individual frames are processed on board where the individual events from each frame are extracted, graded and placed in an event list with a time tag before being staged on board the OSIRIS-REx spacecraft for downlink. The 4 second timing resolution of the detector plane combined with the asteroid rotation period and nominal orbit of OSIRIS-REx during science operations set the lower bounds for the angular resolution of the REXIS instrument at  $3.6'$ , equivalent to a 28 cm spatial resolution on the surface of the asteroid from an altitude of 730 m. The maximum spatial resolution of the detector plane is fixed by the CCD pixel size of  $24 \mu\text{m} \times 24 \mu\text{m}$ , however, since this level of fidelity is not required pixels are re-binned in the on board data processing to super pixels consisting of a  $8 \times 8$  array of native pixels with a pitch of 0.192  $\mu\text{m}$ . This is done primarily to reduce the data volume of the instrument since the full spatial resolution of the detector plane is not required to achieve REXIS's science objectives

Science observations will commence just after the next solar minimum during which time a very low incident solar X-ray flux is expected at the level defined by the Geostationary Operational Environmental Satellite (GOES)

mission A-state, i.e.  $10^{-8}$  W/m<sup>2</sup> in the 1-8 Å band solar X-ray monitor [37]. In order to mitigate this the REXIS field of view has been maximized to enable the collection of as many X-ray events as possible while maintaining minimal exposure to the cosmic X-ray background which is largely obscured by the asteroid in the REXIS field of view. This comes at the expense of reduced spatial resolution on the surface of the asteroid for a collimator based analysis. In an effort to measure elemental abundance with high spatial resolution (26.2') a coded aperture mask with a open hole fraction of 0.5 and pixel pitch of 1.536 mm will be affixed at a distance (focal length) of 20 cm from the surface of the detector plane but reduces the total aperture throughput (see figure 2) by a factor of two. Coded aperture instruments have been used in a variety of astrophysics missions, in particular wide-field hard X-ray monitors sensitive at energies between approximately 15 and 200 keV such as the Swift Burst Alert Telescope (BAT) [38] and the Imager on-board INTEGRAL (IBIS) [39] for the localization, long-term monitoring and characterization of astrophysical point sources. This method was pioneered as a way to image hard X-rays with energies above approximately 10 keV where the use of focusing optics was not possible until recently. In the case of REXIS, which is sensitive between 0.4 and 10 keV, the use of a coded-aperture mask was born primarily out of budget, mass constraints and FOV.

REXIS will be the first application of the coded aperture imaging technique to extended sources. Since the surface being imaged provides the very background against which enhanced emission features are sought, the technique is less sensitive than for point sources (for which it has been traditionally used). However, combined with "collimator mode" imaging (see §8), the coded aperture technique will reveal localized features above some minimum enhancement value. A coded aperture imager operates as a pinhole camera, where additional pinholes have been added in order to increase the total throughput of the instrument. The reconstruction of images from coded aperture instruments proceeds directly from analysis of the X-ray event list by selecting events with the energies within the band of interest then generating detector plane images using the spatial information recorded in the individual CCDs for each exposure. The reconstruction of the local field for each individual exposure is achieved by convolving the detector plane image with the mask image as described in [40] and in §7; this is analogous to a search for the presence of significant projections of the mask pattern on the detector plane from all possible angles in X-rays. A final asteroid image is achieved by co-addition of the individual reconstructed sky images reprojected onto the surface asteroid surface (see §7 for details). Finally the angular resolution of a coded aperture instrument is defined by

$$\delta\phi = \tan^{-1} \left( \frac{\sqrt{p_m^2 + p_d^2}}{f} \right) \quad (1)$$

where  $f$  is the separation between the detector plane and the coded-aperture mask (i.e. focal length),  $p_m$  and  $p_d$  is the pitches of the mask and detector pixels respectively. The angular resolution of the REXIS instrument is 26.2', about a factor of 7.3 below the maximum achievable based on the CCD integration time and the motion of the spacecraft and asteroid. This is equivalent to a spatial resolution on the asteroid surface of 5.6 m at an altitude of 730 m.

## 5. ASTEROID X-RAY EMISSION MODELING

To evaluate the performance of REXIS spectral modeling was carried out primarily using the composition of the nearest meteorite match to the observed spectrum of 101955 Bennu (see §2): that of a C1 chondrite. The single interaction model presented in [41] was adopted and cross checked with an independent GEANT4.3 simulation. The current calculation assumes a smooth spherical asteroid with a uniform density of 1 g/cm<sup>3</sup> (see §2).

The input solar spectrum for baseline simulation was chosen using data from the GOES X-ray monitors [37] in order to estimate the expected temperature and emission measures around the depth of solar minimum, during which REXIS will carry out observations. Using data extracted for the GOES-10 and GOES-12 X-ray monitors averaged over 5 minute intervals and the method introduced in [42] emission measures and temperatures from the time around the previous solar minimum were derived. Taking a simplistic, conservative approach derived emission measures and temperatures from the GOES-10 and GOES-12 satellites were compared and data points found to differ by more than 5% were excluded from consideration. Cumulative probability distributions were calculated for both (see figure 4) and a worst-case scenario temperature 4 MK and an emission measure of  $10^{44}$

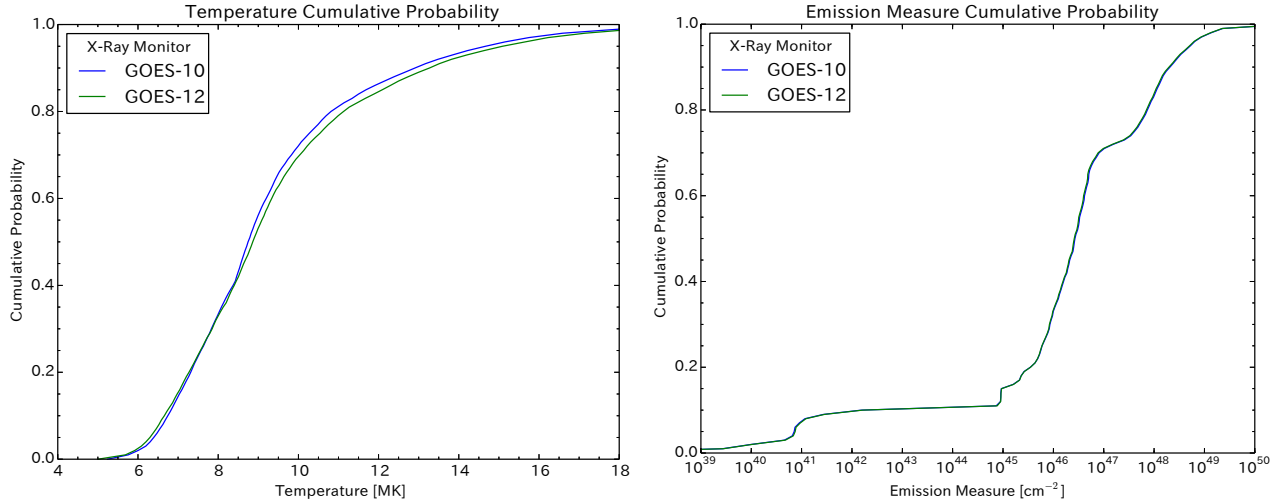


Figure 4: The cumulative probability distribution of the measured temperature and emission measures of the sun using data from the GOES-10, and 12 X-ray monitors during the time around the previous solar minimum between January 1, 2005 and January 1, 2007: the closest analog for the REXIS observing period. A cut on the data has been implemented requiring agreement between the monitor data of 5% in order to exclude instrumental and environmental effects.

$\text{cm}^{-3}$  were adopted and used to generate single temperature models using CHIANTI 7.1 [43, 44]. Additionally these “worst-case” values were compared to results from Reuven Ramatti High Energy Spectroscopic Imager (RHESSI) which place constraints on the solar X-ray spectrum at solar minimum during periods where the GOES 1-8 Å monitors register solar activity below  $10^{-8} \text{ W/m}^2$ , i.e. below the A-state, and found to in be good agreement with this choice of parameters [45]. In addition coronal plasmas at higher temperature states were also considered for the imaging simulation (see §7).

Line	Min. Det. Time
Fe-L	136 sec.
Mg-K	63 sec.
Al-K	7.67 hrs.
Si-K	183 sec.
S-K $\alpha$	5.73 days
Internal bkg. lines not included	

Table 3: The estimated minimum detection times for key elements for an asteroid with the composition of a C1-Chondrite at a significance of  $6\sigma$ .

After calculation of the solar spectrum incident on the asteroid, the induced X-ray fluorescence (XRF) spectrum is derived for a simple spherical asteroid by numerical integration. To accomplish this a map of the asteroid is divided into equal area bins using an AITOFF-Hammer projection, identical to that used in the imaging routines described in §7. The incidence angle and re-emission angle to the position of the OSIRIS-REx spacecraft are derived for each bin then, using the prescription in [41], the coherent and incoherent scattering intensities as well as the intensity of the individual fluorescence lines are calculated. The incoming flux is then integrated over all bins visible to the REXIS instrument weighted by the response function of the coded-aperture mask shown in figure 7a giving the total solar induced XRF spectrum.

In addition the XRF spectrum induced by the cosmic X-ray background (CXB) is calculated in a similar fashion assuming a completely uniform CXB. Under this assumption each bin on the asteroid surface receives the same incident flux from a  $2\pi$  radian region on the sky. Again following [41] but integrating over all possible incidence angles each component of the XRF spectrum is calculated for a fixed spacecraft position giving the total CXB induced XRF spectrum. Combination of these two components give the total predicted count rate for each line of interest during low solar activity incident on the surface of the CCDs. For this time period the CXB induced XRF emission becomes important for elements at energies above 3 to 4 keV. For this calculation particle induced X-ray emission (PIXE) is not yet included but will be incorporated into future models.



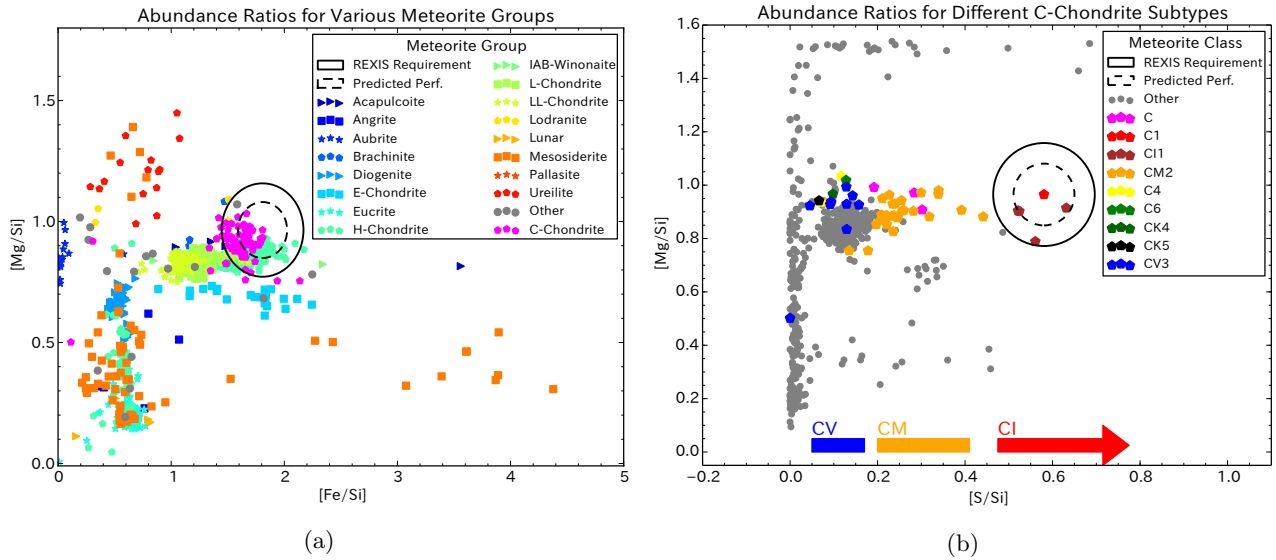


Figure 5: Ground observations have shown Bennu to most closely resemble a C1 or CM chondritic meteorite. Two of the primary objectives of the REXIS mission is to (a) determine whether or not Bennu is indeed a Chondrite, and to (b) determine which type of Chondrite based on observations of Sulfur. The expected performance and requirement values are shown in the above plots for REXIS as a dashed and solid line respectively. The measurements of the elemental abundance ratios for the individual meteorites were carried out in the lab and the results are given in [50].

Next the attenuation due to the presence of the 220 nm thick Al optical blocking filter and due to the presence of organic contaminants on the surface of the CCD is applied along with the quantum efficiency of the detectors as a function of energy (see figure 3) to produce a predicted count rate as a function of energy for the entire REXIS instrument [46]. The collection of contaminants on the surface of the CCD is mitigated by the implementation of pre-flight handling procedures, however the migration and accumulation of organic contaminants on optical blocking filters and detectors consisting primarily of carbon has been observed in both the Chandra X-ray observatory Advanced CCD Imaging Spectrometer (CXO-ACIS) [47], the Suzaku XIS (c.f. [48]) and many others. Such contaminants are suspected to originate from the spacecraft itself [49] with an accumulation rate has been observed to have a strong temperature dependence. Therefore the final contamination properties will vary from mission-to-mission depending upon the components, geometry and temperature of the spacecraft; difficult to assess prior to launch. Based on the observed properties of the CXO-ACIS and Suzaku XIS contamination layers a representative contamination layer consisting of C and O with a atomic ratio C/O=6 and total thickness of  $54 \mu\text{g}/\text{cm}^2$  has been assumed for our simulations. The minimum detection times for elements key to the identification of Bennu outlined in §6 are given in table3.

## 6. METEORITE CLASSIFICATION

The primary objective of the REXIS instrument is the identification 101955 Bennu elemental surface composition through the observation of the Fe-L, Al-K, Mg-K, and Si-K complexes, as well as the S-K $\alpha$  and S-K $\beta$  fluorescence lines. Using data from [50] it was determined that the primary means of identification will be carried out through measurement of the mass abundance ratios [Mg/Si] and [Fe/Si] (see figure 5a) which will enable REXIS to test previous observations of Bennu (see §2). Abundance ratios are typically used in place of simple element abundances as these are relatively insensitive to changes in solar states and unexpected changes in instrument performance. In order to definitively classify Bennu as a carbonaceous chondrite REXIS is required to measure these abundance ratios to within 20% of their true value at a confidence level of  $10\sigma$ ; the current best estimate for the expected performance of the instrument now stands as 18.8% [51].



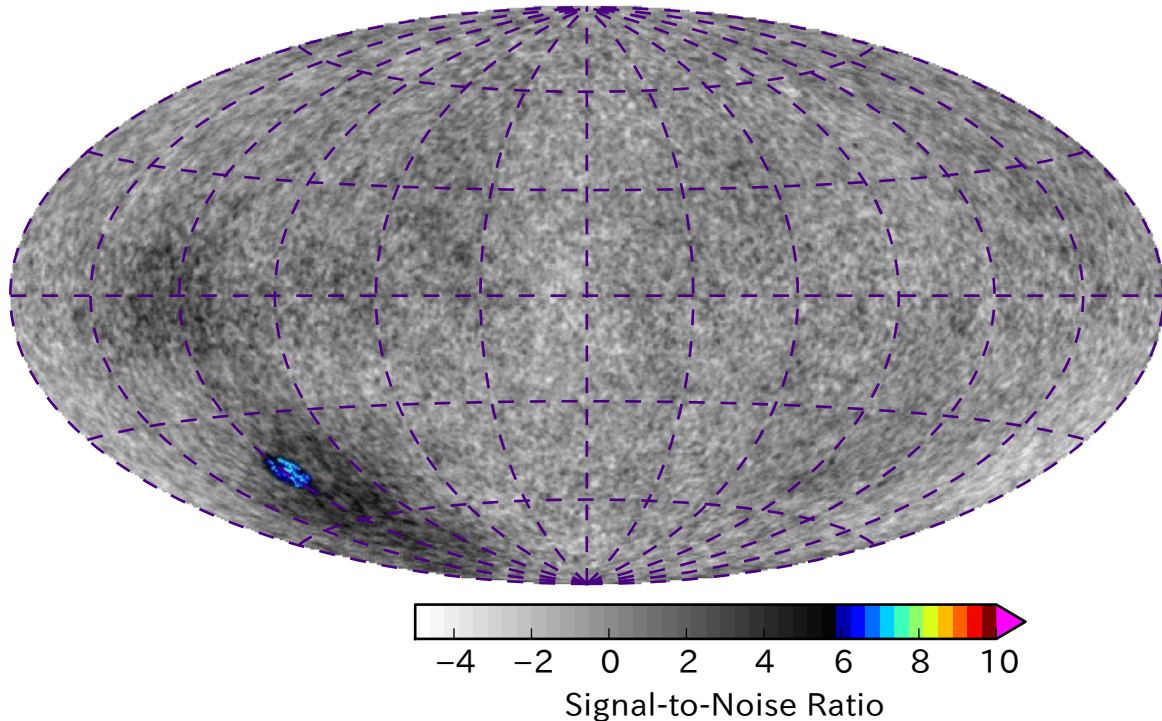


Figure 6: The complete reconstructed, simulated image of Bennu with a single 50 m scale source with a factor of 5 abundance enhancement observed with a total integration time of 20 days. The peak signal-to-noise ratio is 7.8; a simple scaling indicates that a detection at the  $6\sigma$  level is expected for factors of 3.75 enhancement in Fe abundance.

REXIS is not only designed toward determining if Bennu is a carbonaceous chondrite, but will also be able to distinguish the subgroup to which Bennu belongs. To accomplish this the  $[\text{Mg}/\text{Si}]$  and  $[\text{S}/\text{Si}]$  abundance ratios are required to be measured (see figure 5b) to within 20% of their true value with an expected performance of 12%.

## 7. CODED APERTURE IMAGING SIMULATION AND RECONSTRUCTION

An imaging simulation has been carried out for a fixed orbital radius of 1 km around a spherical asteroid with a radius of 280 m in the Fe-L and Mg-K bands in order to assess the sensitivity of the REXIS instrument to enhancements of elemental abundance on 50 m scales on the asteroid surface. Initially a flux map of the asteroid is initially generated on a AITOFF-Hammer equal area projection and regions of enhanced flux are added to the map simulating regions with enhanced elemental abundance.

The imaging simulation proceeds in two step: first the collection of data in 600 second time steps on the detector plane is simulated and a detector plane image generated at each step. This is coarser than the 4 second integration time of the REXIS detector plane (see §3) in order to carry out the simulations within a short time frame: approximately 48 hours for 20 days of simulated observation per CPU core. Next the individual detector plane images are used to reconstruct individual observation images which are then co-added over the surface of the asteroid in a AITOFF-Hammer projection. A search over this final map is then conducted for statistically significant flux enhancement.

The data collection simulation is carried out by initially calculating the sub-solar point and the position of the OSIRIS-REx spacecraft at each step as a function of time fully taking into account the orbit of OSIRIS-REx as well as the rotation of 101955 Bennu. At each simulation step the solar flux incident at each point on the

asteroid is first calculated which is then used to calculate the intensity of the X-ray emission from the surface of the asteroid to the REXIS instrument. The intensity map is then re-projected into the instrument's local field of view on a tangential projection and convolved with the coded aperture mask using a fast Fourier transform (FFT) producing an incident intensity map on the REXIS detector plane. This map is then filtered according to the active area of the CCD and the expectation value of the number of counts in each CCD super-pixel calculated. A simulated observation is then carried out by sampling each pixel on a Poisson distribution using the expectation value producing a single detector plane image. The detector plane image together with the spacecraft position and sub-solar position are stored to disk at each step.

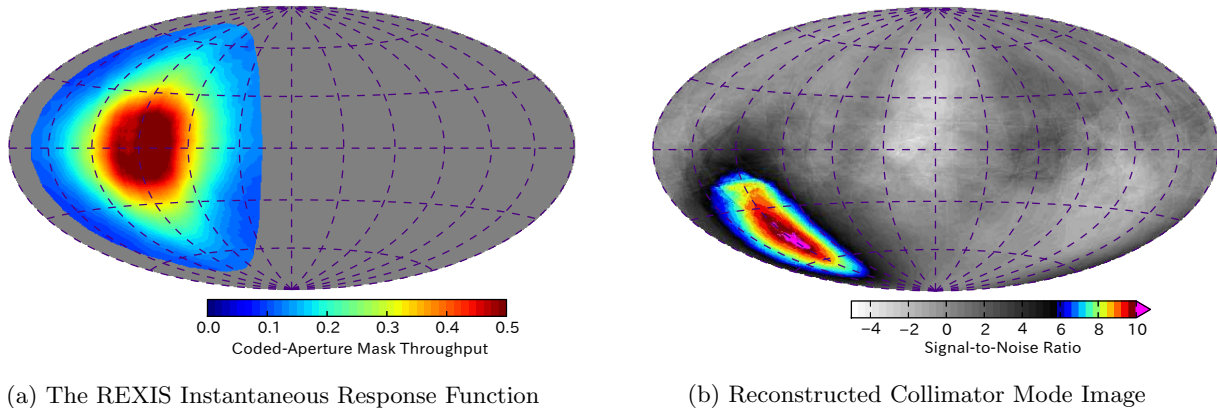
The image reconstruction process is carried out first by reconstructing the sky image from the stored detector plane image through an FFT convolution with the coded-aperture mask using a balanced correlation where open mask pixels are assigned a value of 1 and closed mask pixels are assigned a value of  $\rho/(\rho - 1)$  where  $\rho$  is the open hole fraction [40]; mask pixels outside of the circular mask pattern area are removed from the reconstruction by setting their values to 0. Similarly the sum of all events over all pixels in the detector plane active area is set to 0 by subtraction the mean number of events taken over all active elements. In carrying out this procedure an automatic background subtraction of the reconstructed sky image is carried out giving an excess map in sky coordinates. Using the OSIRIS-REx spacecraft position the sky image is reprojected to asteroid coordinates on an AITOFF-Hammer equal area projection. The equal area projection is used in order to carry out the subsequent analysis on equal sized surface area elements on the asteroid surface as well as to co-add images in a coordinate space that is independent of the spacecraft view factors to the asteroid surface.

In addition a background estimation procedure is also carried out over the asteroid surface by random re-assignment of the positions for individual sky images before re-projection within a fixed time interval around individual images. This time-shuffling procedure has been introduced in order to remove the large-scale anisotropies associated viewing the bright limb of the asteroid and the attendant effect within the co-added sky images in asteroid coordinates. The same goal can be achieved in the detector image space by co-adding detector plane images over a rolling time window to produce a background detector map which can then be subtracted from the individual detector plane before reconstruction of the sky image (see figure 6). Although the variability of the solar flux has not yet been added to this imaging simulation the purpose of a subtracting images at nearby times is to test the procedure that will be required when dealing with long-term variability of the solar state over the REXIS observation period. In the final analysis procedure short-term variability will be handled using input from the SXM to sort individual images into separate solar states for co-addition into separate asteroid maps for each state in order to avoid the appearance of overabundant regions due only to enhanced fluxes caused by solar flares in individual images.

Initially the imaging simulation was carried out assuming a 4 MK coronal temperature with an emission measure of  $10^{44} \text{ cm}^{-2}$ , however it was subsequently determined that the flux enhancements required for the detection of a source on the surface of a C1 Chondrite was unphysical. It was determined shortly thereafter that enhancements Fe and Mg elemental abundance under exposure from a 6 MK sun would yield detectable sources on 50 m scales. Since approximately 95% of observations are likely to be carried under exposure from a  $T \geq 6$  MK sun (see figure 4 and §5) assuming the same conditions as the previous solar minimum: equivalent to 19 days of observation, however intervals of time during which the short wavelength GOES X-ray monitors (0.5-4 Å) were unable to measure significant fluxes from the sun at low solar states were excluded. Assuming these periods represent lower coronal temperatures the expected REXIS observing time during 6 MK solar state requires a downward correction of up to 50%. A more careful evaluation of this is currently underway [52].

## 8. COLLIMATOR MODE SIMULATION AND RECONSTRUCTION

The simulation and reconstruction of images in collimator mode is carried out in a similar manner to that of the imaging simulation and reconstruction described in §7. The key difference is that the response function of the entire REXIS instrument (see figure 7a) is used rather than individual mask pixels for the reconstruction of individual asteroid images. This leads to degraded angular resolution but somewhat higher sensitivity to larger scale elemental abundance enhancements on the asteroid surface. Additionally the terminator orbit configuration for the REXIS observations also proves to be advantageous, particularly for lower energy elements where the



(a) The REXIS Instantaneous Response Function

(b) Reconstructed Collimator Mode Image

Figure 7: (a) The response function of the REXIS instrument is defined by the coded aperture mask throughput shown for REXIS during nadir pointing at  $(lat, lon) = (-90.0, 0.0)$ . For reconstruction of elemental abundance maps at low energies the response function can be further reduced by weighting the exposed areas by the intensity of the solar exposure. (b) The reconstructed image of elemental abundance enhancements for a single Fe enhancement located on the surface of 101955 Bennu identical to that detected in figure 6. The peak signal to noise of the detected source  $10.2\sigma$ .

relative contribution of the CXB induced X-ray fluorescence is low and the emission can be approximately considered to originate from one half of the REXIS field of view.

In order to simulate the collimator mode reconstruction the same simulated data set consisting of detector plane images, the OSIRIS-REx spacecraft position, and sub-solar position as a function of time is generated as described in §7. The position of each detector plane image is then used to project the collimator response function onto the surface of the asteroid weighted by the total number of events registered in the detector plane over the energy band of interest. For low energy elements whose fluorescence lines are primarily induced by solar X-ray the emission can be considered to have originated from the illuminated half of the asteroid. Weighting of the response function by the incident solar exposure, effectively cutting the response function in half, improves the collimator mode spatial resolution by approximately a factor of two.

A similar method for the estimation of a background map is also carried out by time shuffling collimator and co-adding images on the asteroid surface as was described in §7. As before a time window of 12000 seconds, equivalent to 20 exposures, was adopted. After generation the raw asteroid map is subtracted from the background asteroid map giving excess as a function of position with a spatial resolution on the asteroid surface of 250 m.

Studies are underway to further characterize the performance of this reconstruction technique for the REXIS instrument as a function of source strength and extension [52], however low spatial resolution detections of source on the asteroid surface have been simulated resulting in high signal-to-noise detections for Fe sources on scales of 50 m and larger with a factor of 5 element abundance enhancement (c.f. figure 7b).

## 9. OPTIMIZATION OF THE REXIS IMAGING SYSTEM

The REXIS instrument (see figure 2) coded aperture mask and imaging system has been optimized using the imaging simulation described in §7. The primary parameters for optimization were the radius of the mask pattern, the mask open hole fraction, and the pixel pitch of the mask as well as that of the detector plane; see table 2 for a list of the current parameters.

The optimization procedure was as follows: the input parameters for a candidate mask are set, i.e. pattern radius, pixel pitch, support grid width, and open hole fraction, each mask pattern was optimized through generation of 1000 candidate masks. Next a extreme high flux point source simulation using the REXIS detector plane with a pixel pitch of 0.368 mm and iterating the source over the entire REXIS field of view in order

to measure the maximum achievable signal-to-noise ratio. From the sample of 1000 candidate masks the mask showing the best performance over the entire field of view is chosen for use in the subsequent simulations discussed below.

The first parameter considered for optimization was the mask and detector plane pixel pitch. A series of simulations for the full observation period of REXIS was carried out for a test detector with pixel pitch of 0.368 mm and a mask pixel pitch of 1.152 mm with a region of enhancement identical to that described in §7. This leads to an improvement in the angular resolution from 26.2' to 20.7' at the cost of a 7% decrease in the total count rate resulting from a decrease in the mask throughput. This is due to the chemical etching process used for the production of the coded aperture mask which requires that the support grids running between individual elements are at least equal to the thickness of the material; in this case 100  $\mu\text{m}$ . The on-axis throughput of a coded aperture mask with support grids can be calculated by  $T' = T(1 - g/m_p)^2$ , where  $T$  is the throughput expected for a perfect mask without support grids, i.e. the open hole fraction,  $m_p$  is the mask pixel pitch and  $g$  is the width of the support grid. For the test carried out here a 4.8% decrease in the on-axis throughput, from 0.437 to 0.417, occurs in the transition from the 1.536 mm mask to the 1.152 mm mask. Although this will not have a significant negative impact on our observations the 1.536 mm mask was retained since a significant positive impact was also not observed. From a fabrication and integration perspective the tightening of the alignment requirements for the use of the finer pitch mask was not warranted given the lack of any clear advantage.

It was recognized early on that the performance of the spectral observations could be improved by increasing the throughput of the coded aperture mask at the expense of imaging sensitivity. In order to ascertain the effects on imaging the same simulation was run using coded aperture masks with ideal open fractions of 0.25, 0.35, 0.4, 0.6, 0.65, and 0.75. A series of 10 simulations were run for each mask pattern in order to measure not only the peak signal-to-noise ratio of each source but also to check the fluctuation level of the result. No significant detections were found in any of these test runs. Additional simulation were initiated for masks with open fraction of 0.45 and 0.55 in a search for potential optimization of the image reconstruction unfortunately the result here was also negative, confirming the open hole fraction of 0.5 to be optimal for the observation of Benu.

## 10. DISCUSSION

The REXIS instrument has been optimized for observation of the near-Earth asteroid 101955 Benu as part of the OSIRIS-REx mission and seeks to identify a meteorite classification of Benu through measurement of elemental abundances by observation of solar X-ray and CXB induced fluorescence lines emitted from the surface of the asteroid. REXIS will also search for localized areas of enhanced elemental abundance with scale sizes of approximately 50 m in order to aid in the selection of a sample collection site using a coded aperture mask capable of resolving features as small as 5.6 m on the surface of the asteroid. REXIS will be the first instrument to employ this technique for use on a planetary mission and owing to its large field of view will also maintain similar capabilities to instruments which have previously been used in this capacity.

## ACKNOWLEDGMENTS

This work was supported under NASA Grants NNX12AG65G and NNG12FD70C. We would like to thank Martin Elvis for making the initial contact between the Harvard College Observatory and Massachusetts Institute of Technology groups which have participated in the development of REXIS, Lucy Lim for providing invaluable advice on the utility of solar X-ray monitors, George Sondecker for his work during the proposal and early phase of this project, as well as Kevin Ryu and Vsyhi Suntharalingam for the preparation of the REXIS CCDs.

## References

- [1] D. S. Lauretta and OSIRIS-Rex Team, "An Overview of the OSIRIS-REx Asteroid Sample Return Mission," in *Lunar and Planetary Institute Science Conference Abstracts, Lunar and Planetary Institute Science Conference Abstracts* **43**, p. 2491, Mar. 2012. [1](#)

- [2] W. V. Boynton, D. S. Lauretta, E. Beshore, O. Barnouin, E. B. Bierhaus, R. Binzel, P. R. Christensen, M. Daly, J. Grindlay, V. Hamilton, A. R. Hildebrand, G. Mehall, D. Reuter, B. Rizk, A. Simon-Miller, and P. S. Smith, "The OSIRIS-REx mission to RQ36: nature of the remote sensing observations," in *European Planetary Science Congress 2012*, p. 875, Sept. 2012. [1](#)
- [3] P. H. Smith, B. Rizk, E. Kinney-Spano, C. Fellows, C. d'Aubigny, and C. Merrill, "The OSIRIS-REx Camera Suite (OCAMS)," *LPI Contributions* **1719**, p. 1690, Mar. 2013. [1](#)
- [4] C. S. Dickinson, M. Daly, O. Barnouin, B. Bierhaus, D. Gaudreau, J. Tripp, M. Ilnicki, and A. Hildebrand, "An Overview of the OSIRIS REx Laser Altimeter (OLA)," in *Lunar and Planetary Institute Science Conference Abstracts, Lunar and Planetary Institute Science Conference Abstracts* **43**, p. 1447, Mar. 2012. [1](#)
- [5] A. A. Simon-Miller and D. C. Reuter, "OSIRIS-REx OVIRS: A Scalable Visible to Near-IR Spectrometer for Planetary Study," *LPI Contributions* **1719**, p. 1100, Mar. 2013. [1](#)
- [6] D. C. Reuter and A. A. Simon-Miller, "The OVIRS Visible/IR Spectrometer on the OSIRIS-Rex Mission," *LPI Contributions* **1683**, p. 1074, Oct. 2012. [1](#)
- [7] G. H. Stokes, J. B. Evans, H. E. M. Viggh, F. C. Shelly, and E. C. Pearce, "Lincoln Near-Earth Asteroid Program (LINEAR)," *Icarus* **148**, pp. 21–28, Nov. 2000. [2](#)
- [8] S. R. Chesley, P. W. Chodas, A. Milani, G. B. Valsecchi, and D. K. Yeomans, "Quantifying the risk posed by potential earth impacts," *Icarus* **159**(2), pp. 423 – 432, 2002. [2](#)
- [9] "Near Earth Object Program, Sentry Risk Table," September 7, 2013. Retrieved: <http://neo.jpl.nasa.gov/risk/index.html>. [2](#)
- [10] M. C. Nolan, C. Magri, E. S. Howell, L. A. Benner, J. D. Giorgini, C. W. Hergenrother, R. S. Hudson, D. S. Lauretta, J.-L. Margot, S. J. Ostro, and D. J. Scheeres, "Shape model and surface properties of the OSIRIS-REx target Asteroid (101955) Bennu from radar and lightcurve observations," *Icarus* **226**(1), pp. 629 – 640, 2013. [2](#)
- [11] C. W. Hergenrother, M. C. Nolan, R. P. Binzel, E. A. Cloutis, M. A. Barucci, P. Michel, D. J. Scheeres, C. D. d'Aubigny, D. Lazzaro, N. Pinilla-Alonso, H. Campins, J. Licandro, B. E. Clark, B. Rizk, E. C. Beshore, and D. S. Lauretta, "Lightcurve, Color and Phase Function Photometry of the OSIRIS-REx Target Asteroid (101955) Bennu," *Icarus* **226**, pp. 663–670, Sept. 2013. [2](#)
- [12] B. E. Clark, R. P. Binzel, E. S. Howell, E. A. Cloutis, M. Ockert-Bell, P. Christensen, M. A. Barucci, F. DeMeo, D. S. Lauretta, H. C. Jr., A. Soderberg, C. Hergenrother, L. Lim, J. Emery, and M. Mueller, "Asteroid (101955) 1999 RQ36: Spectroscopy from 0.4 to 2.4 $\mu$ m and meteorite analogs," *Icarus* **216**(2), pp. 462 – 475, 2011. [3](#)
- [13] I. Adler, J. Trombka, J. Gerard, R. Schmadebeck, P. Lowman, H. Blodget, L. Yin, E. Eller, R. Lamothe, P. Gorenstein, P. Bjorkholm, B. Harris, and H. Gursky, *Apollo 15: Preliminary Science Report. NASA SP-289*, vol. 289 of *NASA Special Publication*, 1972. [3](#)
- [14] I. Adler, J. Gerard, J. Trombka, R. Schmadebeck, P. Lowman, H. Blodget, L. Yin, E. Eller, R. Lamothe, P. Gorenstein, P. Bjorkholm, B. Harris, and H. Gursky, "The Apollo 15 x-ray fluorescence experiment," in *Lunar and Planetary Science Conference Proceedings*, A. E. Metzger, J. I. Trombka, L. E. Peterson, R. C. Reedy, and J. R. Arnold, eds., *Lunar and Planetary Science Conference Proceedings* **3**, p. 2157, 1972. [3](#), [4](#)
- [15] T. Okada, K. Shirai, Y. Yamamoto, T. Arai, K. Ogawa, H. Shiraishi, M. Iwasaki, T. Kawamura, H. Morito, M. Kato, and Selene Xrs Team, "X-Ray Fluorescence Experiments on the SELENE (Kaguya) Spacecraft," in *Lunar and Planetary Institute Science Conference Abstracts, Lunar and Planetary Inst. Technical Report* **39**, p. 1960, Mar. 2008. [3](#), [5](#)



- [16] M. Kato, S. Sasaki, and Y. Takizawa, "The Kaguya Mission Overview," *Space Sci. Rev.* **154**, pp. 3–19, July 2010. [5](#)
- [17] T. Okada, K. Shirai, Y. Yamamoto, T. Arai, K. Ogawa, H. Shiraiishi, M. Iwasaki, T. Kawamura, H. Morito, M. Grande, and M. Kato, "X-Ray Fluorescence Spectrometry of Lunar Surface by XRS Onboard SELENE (Kaguya)," *Transactions of Space Technology Japan* **7**, pp. 39–, 2010. [3](#)
- [18] T. Okada, M. Kato, A. Fujimura, H. Tsunemi, and S. Kitamoto, "X-ray fluorescence spectrometer onboard Muses-C," *Advances in Space Research* **25**, pp. 345–348, 2000. [3](#)
- [19] T. Okada, M. Kato, K. Shirai, Y. Yamamoto, T. Matsuda, H. Tsunemi, and S. Kitamoto, "Elemental mapping of asteroid 1989ML from MUSES-C orbiter," *Advances in Space Research* **29**, pp. 1237–1242, 2002. [5](#)
- [20] T. Okada, K. Shirai, Y. Yamamoto, T. Arai, K. Ogawa, K. Hosono, and M. Kato, "X-ray Fluorescence Spectrometry of Asteroid Itokawa by Hayabusa," *Science* **312**, pp. 1338–1341, June 2006. [3](#), [5](#)
- [21] C. Howe, D. Drummond, R. Edeson, B. Maddison, D. Parker, R. Parker, A. Shrivastava, J. Spencer, B. Kellett, M. Grande, P. Sreekumar, J. Huovelin, D. Smith, J. Gow, S. N. K.C., and L. dUston, "Chandrayaan-1 X-ray Spectrometer (C1XS) Instrument design and technical details," *Planetary and Space Science* **57**(7), pp. 735 – 743, 2009. [3](#), [5](#)
- [22] S. Narendranath, P. Athiray, P. Sreekumar, B. Kellett, L. Alha, C. Howe, K. Joy, M. Grande, J. Huovelin, I. Crawford, U. Unnikrishnan, S. Lalita, S. Subramaniam, S. Weider, L. Nittler, O. Gasnault, D. Rothery, V. Fernandes, N. Bhandari, J. Goswami, and M. Wiczorek, "Lunar X-ray fluorescence observations by the Chandrayaan-1 X-ray Spectrometer (C1XS): Results from the nearside southern highlands," *Icarus* **214**(1), pp. 53 – 66, 2011. [3](#), [5](#)
- [23] M. Grande, R. Browning, N. Waltham, D. Parker, S. Dunkin, B. Kent, B. Kellett, C. Perry, B. Swinyard, A. Perry, J. Feraday, C. Howe, G. McBride, K. Phillips, J. Huovelin, P. Muhli, P. Hakala, O. Vilhu, J. Laukkanen, N. Thomas, D. Hughes, H. Alleyne, M. Grady, R. Lundin, S. Barabash, D. Baker, P. Clark, C. Murray, J. Guest, I. Casanova, L. d'Uston, S. Maurice, B. Foing, D. Heather, V. Fernandes, K. Muinonen, S. Russell, A. Christou, C. Owen, P. Charles, H. Koskinen, M. Kato, K. Sipila, S. Nenonen, M. Holmstrom, N. Bhandari, R. Elphic, and D. Lawrence, "The d-cixs x-ray mapping spectrometer on smart-1," *Planetary and Space Science* **51**(6), pp. 427 – 433, 2003. [3](#), [4](#)
- [24] L. R. Nittler, R. D. Starr, L. Lim, T. J. McCoy, T. H. Burbine, R. C. Reedy, J. I. Trombka, P. Gorenstein, S. W. Squyres, W. V. Boynton, T. P. McClanahan, J. S. Bhangoo, P. E. Clark, M. E. Murphy, and R. Killen, "X-ray fluorescence measurements of the surface elemental composition of asteroid 433 Eros," *Meteoritics and Planetary Science* **36**, pp. 1673–1695, Dec. 2001. [3](#), [5](#)
- [25] C. E. Schlemm, R. D. Starr, G. C. Ho, K. E. Bechtold, S. A. Hamilton, J. D. Boldt, W. V. Boynton, W. Bradley, M. E. Fraeman, R. E. Gold, J. O. Goldsten, J. R. Hayes, S. E. Jaskulek, E. Rossano, R. A. Rumpf, E. D. Schaefer, K. Strohbehn, R. G. Shelton, R. E. Thompson, J. I. Trombka, and B. D. Williams, "The X-Ray Spectrometer on the MESSENGER Spacecraft," *Space Sci. Rev.* **131**, pp. 393–415, Aug. 2007. [3](#)
- [26] L. R. Nittler, R. D. Starr, S. Z. Weider, T. J. McCoy, W. V. Boynton, D. S. Ebel, C. M. Ernst, L. G. Evans, J. O. Goldsten, D. K. Hamara, D. J. Lawrence, R. L. McNutt, C. E. Schlemm, S. C. Solomon, and A. L. Sprague, "The Major-Element Composition of Mercury's Surface from MESSENGER X-ray Spectrometry," *Science* **333**, pp. 1847–, Sept. 2011. [3](#), [5](#)
- [27] G. W. Fraser, J. D. Carpenter, D. A. Rothery, J. F. Pearson, A. Martindale, J. Huovelin, J. Treis, M. Anand, M. Anttila, M. Ashcroft, J. Benkoff, P. Bland, A. Bowyer, A. Bradley, J. Bridges, C. Brown, C. Bulloch, E. J. Bunce, U. Christensen, M. Evans, R. Fairbend, M. Feasey, F. Giannini, S. Hermann, M. Hesse, M. Hilchenbach, T. Jorden, K. Joy, M. Kaipiainen, I. Kitchingman, P. Lechner, G. Lutz, A. Malkki, K. Muinonen,



- J. Näränen, P. Portin, M. Prydderch, J. S. Juan, E. Sclater, E. Schyns, T. J. Stevenson, L. Strüder, M. Syrajasuo, D. Talboys, P. Thomas, C. Whitford, and S. Whitehead, “The mercury imaging X-ray spectrometer (MIXS) on bepicolombo,” *Planet. Space Sci.* **58**, pp. 79–95, Jan. 2010. [3](#), [5](#)
- [28] J. Treis, L. Andricek, F. Aschauer, K. Heinzinger, S. Herrmann, M. Hilchenbach, T. Lauf, P. Lechner, G. Lutz, P. Majewski, M. Porro, R. H. Richter, G. Schaller, M. Schnecke, F. Schopper, H. Soltau, A. Stefanescu, L. Strüder, and G. de Vita, “MIXS on BepiColombo and its DEPFET based focal plane instrumentation,” *Nuclear Instruments and Methods in Physics Research A* **624**, pp. 540–547, Dec. 2010. [3](#), [5](#)
- [29] I. Crawford, K. Joy, B. Kellett, M. Grande, M. Anand, N. Bhandari, A. Cook, L. dUston, V. Fernandes, O. Gasnault, J. Goswami, C. Howe, J. Huovelin, D. Koschny, D. Lawrence, B. Maddison, S. Maurice, S. Narendranath, C. Pieters, T. Okada, D. Rothery, S. Russell, P. Sreekumar, B. Swinyard, M. Wiczorek, and M. Wilding, “The scientific rationale for the C1XS X-ray spectrometer on India’s Chandrayaan-1 mission to the moon,” *Planetary and Space Science* **57**(7), pp. 725 – 734, 2009. [5](#)
- [30] K. Koyama, H. Tsunemi, T. Dotani, M. W. Bautz, K. Hayashida, T. G. Tsuru, H. Matsumoto, Y. Ogawara, G. R. Ricker, J. Doty, S. E. Kissel, R. Foster, H. Nakajima, H. Yamaguchi, H. Mori, M. Sakano, K. Hamaguchi, M. Nishiuchi, E. Miyata, K. Torii, M. Namiki, S. Katsuda, D. Matsuura, T. Miyauchi, N. Anabuki, N. Tawa, M. Ozaki, H. Murakami, Y. Maeda, Y. Ichikawa, G. Y. Prigozhin, E. A. Boughan, B. Lamarr, E. D. Miller, B. E. Burke, J. A. Gregory, A. Pillsbury, A. Bamba, J. S. Hiraga, A. Senda, H. Katayama, S. Kitamoto, M. Tsujimoto, T. Kohmura, Y. Tsuboi, and H. Awaki, “X-Ray Imaging Spectrometer (XIS) on Board Suzaku,” *PASJ* **59**, pp. 23–33, Jan. 2007. [5](#)
- [31] K. Mitsuda, M. Bautz, H. Inoue, R. L. Kelley, K. Koyama, H. Kunieda, K. Makishima, Y. Ogawara, R. Petre, T. Takahashi, H. Tsunemi, N. E. White, N. Anabuki, L. Angelini, K. Arnaud, H. Awaki, A. Bamba, K. Boyce, G. V. Brown, K.-W. Chan, J. Cottam, T. Dotani, J. Doty, K. Ebisawa, Y. Ezoe, A. C. Fabian, E. Figueroa, R. Fujimoto, Y. Fukazawa, T. Furusho, A. Furuzawa, K. Gendreau, R. E. Griffiths, Y. Haba, K. Hamaguchi, I. Harrus, G. Hasinger, I. Hatsukade, K. Hayashida, P. J. Henry, J. S. Hiraga, S. S. Holt, A. Hornschemeier, J. P. Hughes, U. Hwang, M. Ishida, Y. Ishisaki, N. Isobe, M. Itoh, N. Iyomoto, S. M. Kahn, T. Kamae, H. Katagiri, J. Kataoka, H. Katayama, N. Kawai, C. Kilbourne, K. Kinugasa, S. Kissel, S. Kitamoto, M. Kohama, T. Kohmura, M. Kokubun, T. Kotani, J. Kotoku, A. Kubota, G. M. Madejski, Y. Maeda, F. Makino, A. Markowitz, C. Matsumoto, H. Matsumoto, M. Matsuoka, K. Matsushita, D. McCammon, T. Mihara, K. Misaki, E. Miyata, T. Mizuno, K. Mori, H. Mori, M. Morii, H. Moseley, K. Mukai, H. Murakami, T. Murakami, R. Mushotzky, F. Nagase, M. Namiki, H. Negoro, K. Nakazawa, J. A. Nousek, T. Okajima, Y. Ogasaka, T. Ohashi, T. Oshima, N. Ota, M. Ozaki, H. Ozawa, A. N. Parmar, W. D. Pence, F. S. Porter, J. N. Reeves, G. R. Ricker, I. Sakurai, W. T. Sanders, A. Senda, P. Serlemitsos, R. Shibata, Y. Soong, R. Smith, M. Suzuki, A. E. Szymkowiak, H. Takahashi, T. Tamagawa, K. Tamura, T. Tamura, Y. Tanaka, M. Tashiro, Y. Tawara, Y. Terada, Y. Terashima, H. Tomida, K. Torii, Y. Tsuboi, M. Tsujimoto, T. G. Tsuru, M. J. L. . Turner, Y. Ueda, S. Ueno, M. Ueno, S. Uno, Y. Urata, S. Watanabe, N. Yamamoto, K. Yamaoka, N. Y. Yamasaki, K. Yamashita, M. Yamauchi, S. Yamauchi, T. Yaqoob, D. Yonetoku, and A. Yoshida, “The X-Ray Observatory Suzaku,” *PASJ* **59**, pp. 1–7, Jan. 2007. [5](#)
- [32] M. W. Bautz, S. E. Kissel, G. Y. Prigozhin, B. LaMarr, B. E. Burke, and J. A. Gregory, “Progress in x-ray CCD sensor performance for the Astro-E2 X-ray imaging spectrometer,” in *Society of Photo-Optical Instrumentation Engineers (SPIE) Conference Series*, A. D. Holland, ed., *Society of Photo-Optical Instrumentation Engineers (SPIE) Conference Series* **5501**, pp. 111–122, Sept. 2004. [5](#)
- [33] M. W. Bautz, S. E. Kissel, B. J. LaMarr, and G. Y. Prigozhin, “Improved x-ray CCD response at very low x-ray energies,” in *Society of Photo-Optical Instrumentation Engineers (SPIE) Conference Series*, *Society of Photo-Optical Instrumentation Engineers (SPIE) Conference Series* **6266**, July 2006. [5](#)
- [34] K. C. Gendreau, Z. Arzoumanian, and T. Okajima, “The Neutron star Interior Composition Explorer (NICER): an Explorer mission of opportunity for soft x-ray timing spectroscopy,” in *Society of Photo-Optical Instrumentation Engineers (SPIE) Conference Series*, *Society of Photo-Optical Instrumentation Engineers (SPIE) Conference Series* **8443**, Sept. 2012. [6](#)

- [35] G. Prigozhin, K. Gendreau, R. Foster, G. Ricker, J. Villaseñor, J. Doty, S. Kenyon, Z. Arzoumanian, R. Redus, and A. Huber, "Characterization of the silicon drift detector for NICER instrument," in *Society of Photo-Optical Instrumentation Engineers (SPIE) Conference Series, Society of Photo-Optical Instrumentation Engineers (SPIE) Conference Series* **8453**, July 2012. [6](#)
- [36] R. Redus, A. Huber, J. Pantazis, and T. Pantazis, "Enhanced energy range thermoelectrically cooled silicon x-ray detectors," in *Nuclear Science Symposium and Medical Imaging Conference (NSS/MIC), 2011 IEEE*, pp. 580–585, 2011. [6](#)
- [37] F. A. Hanser and F. B. Sellers, "Design and calibration of the GOES-8 solar x-ray sensor: the XRS," *Proc. SPIE* **2812**, pp. 344–352, 1996. [7](#)
- [38] S. D. Barthelmy, L. M. Barbier, J. R. Cummings, E. E. Fenimore, N. Gehrels, D. Hullinger, H. A. Krimm, C. B. Markwardt, D. M. Palmer, A. Parsons, G. Sato, M. Suzuki, T. Takahashi, M. Tashiro, and J. Tueller, "The Burst Alert Telescope (BAT) on the SWIFT Midex Mission," *Space Sci. Rev.* **120**, pp. 143–164, Oct. 2005. [7](#)
- [39] P. Ubertini, F. Lebrun, G. Di Cocco, A. Bazzano, A. J. Bird, K. Broenstad, A. Goldwurm, G. La Rosa, C. Labanti, P. Laurent, I. F. Mirabel, E. M. Quadrini, B. Ramsey, V. Reglero, L. Sabau, B. Sacco, R. Staubert, L. Vigroux, M. C. Weisskopf, and A. A. Zdziarski, "IBIS: The Imager on-board INTEGRAL," *A&A* **411**, pp. L131–L139, Nov. 2003. [7](#)
- [40] E. E. Fenimore and T. M. Cannon, "Coded aperture imaging with uniformly redundant arrays," *Appl. Opt.* **17**, pp. 337–347, Feb. 1978. [7](#), [11](#)
- [41] P. E. Clark and J. I. Trombka, "Remote X-ray spectrometry for NEAR and future missions: Modeling and analyzing X-ray production from source to surface," *J. Geophys. Res.* **102**, pp. 16361–16384, July 1997. [7](#), [8](#)
- [42] S. M. White, R. J. Thomas, and R. A. Schwartz, "Updated Expressions for Determining Temperatures and Emission Measures from Goes Soft X-Ray Measurements," *Sol. Phys.* **227**, pp. 231–248, Apr. 2005. [7](#)
- [43] K. P. Dere, E. Landi, H. E. Mason, B. C. Monsignori Fossi, and P. R. Young, "CHIANTI - an atomic database for emission lines," *A&AS* **125**, pp. 149–173, Oct. 1997. [8](#)
- [44] E. Landi, P. R. Young, K. P. Dere, G. Del Zanna, and H. E. Mason, "CHIANTI—An Atomic Database for Emission Lines. XIII. Soft X-Ray Improvements and Other Changes," *ApJ* **763**, p. 86, Feb. 2013. [8](#)
- [45] I. G. Hannah, G. J. Hurford, H. S. Hudson, R. P. Lin, and K. van Bibber, "First Limits on the 3-200 keV X-Ray Spectrum of the Quiet Sun Using RHESSI," *ApJ* **659**, pp. L77–L80, Apr. 2007. [8](#)
- [46] B. Allen *et al.*, "Modeling the X-Ray Spectrum of 101955 Bennu for REXIS," 2014. In Preparation. [9](#)
- [47] P. P. Plucinsky, N. S. Schulz, H. L. Marshall, C. E. Grant, G. Chartas, D. Sanwal, M. Teter, A. A. Vikhlinin, R. J. Edgar, M. W. Wise, G. E. Allen, S. N. Virani, J. M. DePasquale, and M. T. Raley, "Flight spectral response of the ACIS instrument," in *Society of Photo-Optical Instrumentation Engineers (SPIE) Conference Series*, J. E. Truemper and H. D. Tananbaum, eds., *Society of Photo-Optical Instrumentation Engineers (SPIE) Conference Series* **4851**, pp. 89–100, Mar. 2003. [9](#)
- [48] "XIS Contamination Monitoring Page." <http://space.mit.edu/XIS/monitor/contam/>. [9](#)
- [49] M. W. Bautz. "Private Communication", 09 2013. [9](#)
- [50] L. R. Nittler, T. J. McCoy, P. E. Clark, M. E. Murphy, J. I. Trombka, and E. Jarosewich, "Bulk element compositions of meteorites: A guide for interpreting remote-sensing geochemical measurements of planets and asteroids," *Antarctic Meteorite Research* **17**, p. 231, 2004. [9](#)
- [51] K. N. Inamdar *et al.*, "Global Element Abundance Reconstruction with the REgolith X-Ray Imaging Spectrometer (REXIS)," 2014. In Preparation. [9](#)
- [52] B. Allen *et al.*, "Imaging Elemental Abundance Enhancements on the Surface of Asteroids," 2014. In Preparation. [11](#), [12](#)